Multicomponent Organic Nanoparticles for Fluorescence Studies in Biological Systems

Tom O. McDonald, Philip Martin, Joseph P. Patterson, Darren Smith, Marco Giardiello, Marco Marcello, Violaine See, Rachel K. O'Reilly, Andrew Owen, and Steve Rannard**

The formation of dual-component organic nanoparticles by a modified emulsion-templated freeze-drying approach leads to aqueous nanosuspensions showing fluorescence (Förster) resonance energy transfer (FRET) from within a distribution of single nanoparticles. The combination of both FRET dyes within dual-component nanoparticles (<200 nm) allows the spatial and physical monitoring of the particles, as the FRET signal is lost on dissolution and breakdown of the nanoparticles. The monitoring of accumulation by Caco-2 cells and macrophages shows very limited internalization within the non-phagocytic cells. Conservation of FRET within the macrophages confirms extensive whole-particle internalization. The cellular permeability through Caco-2 monolayers is also assessed and movement of intact dual-component particles is observed, suggesting a mechanism for enhanced pharmacokinetics in vivo.

1. Introduction

The use of nanosuspensions, particles of pure drug in the submicrometer size range,[1] has been heralded as an approach to address the issue of formulating poorly soluble active pharmaceutical ingredients (API)[2–9] and has been successful in producing a range of new medicines, dosed daily in clinics globally. These include the immunosuppressant Rapamune (rapamycin), the chemotherapy-induced nausea prevention medicine Emend (aprepitant), and the hypercholesterolemia treatment TriCor (fenofibrate). The solid drug particles do not utilize a drug carrier or a drug vehicle such as vesicles, micelles, or pegylation[10] to overcome poor solubility, therefore each particle conveys high drug content, offering an efficient way to deliver drugs to and/or into cells. Additionally, formulating a poorly soluble drug as a nanosuspension has been shown to enhance dissolution rate and improve bioavailability[7,11,12] over conventional drug formulation approaches.

The in vivo behavior of drugs in various nanoparticle forms has been subject to a considerable amount of research.[13–15] Ongoing study continues to investigate the cellular uptake and accumulation of a wide range of nanoparticles, nanoparticulate drug delivery systems, and colloidal particles with a specific emphasis on toxicity.[14,16] Nanosuspensions, typically composed of aggregates or crystals of poorly soluble organic molecules, have a finite solubility and do not utilize a nanoscopic vehicle for delivery, therefore the nanoparticles will undergo continuous dissolution within the body.

The Caco-2 cell line, originating from human colorectal carcinoma, has been shown to spontaneously differentiate in culture to form a confluent monolayer with morphological and functional similarities to the small intestinal epithelium.[17] As a result of these characteristics the Caco-2 monolayer has been developed as a model to study a range of therapeutic agents and delivery vehicles (microparticles,[18] nanoparticles,[19] and nanocomplexes[20]). Hu and co-workers compared the uptake into Caco-2 cells (human intestinal, non-phagocytic) and phagocytic cells (mouse macrophage RAW cells) of charcoal nanoparticles and a pyrene nanosuspension using optical microscopy.[21] Both types of particle displayed similar uptake behavior; limited in the Caco-2 cells but extensive in the RAW cells. The limitations of optical microscopy led to a lack of clarity regarding whether the pyrene particles were indeed internalized intact or transported as dissolved molecules with subsequent accumulation within the cell. Other studies have shown that nanosuspensions of hydrophobic drugs, produced by milling, gave an increase in the apparent permeability through a Caco-2 monolayer compared to un-milled drug. The authors suggested that improvement of oral bioavailability was due to increased dissolution rather than movement of particles through the cells of the gastrointestinal (GI) tract.[2] The transport and fate of nanosuspensions within the body is therefore relatively poorly understood with respect to: a) whether particles, when orally dosed, cross

Dr. T. O. McDonald, Dr. M. Giardiello, Prof. S. Rannard
Department of Chemistry
University of Liverpool
Crown Street, Liverpool, L69 7ZD, UK
E-mail: srannard@liv.ac.uk
Dr. P. Martin, Dr. D. Smith, Prof. A. Owen
Department of Molecular and Clinical, Pharmacology
University of Liverpool
Block H, 70 Pembroke Place, Liverpool, L69 3GF, UK
E-mail: aowen@liv.ac.uk
J. P. Patterson, Dr. R. K. O'Reilly
University of Warwick
Department of Chemistry
Gibbet Hill Road, Coventry, CV4 7AL, UK
Dr. M. Marcello, Dr. V. See
Centre for Cell Imaging
Institute of Integrative Biology
University of Liverpool
Liverpool, L69 7ZB, UK

DOI: 10.1002/adfm.201103059

the GI tract and enter the circulation intact; b) whether dissolution occurs before cellular uptake; and c) whether particles remain intact over considerable timescales after uptake into phagocytic cells. Accurate monitoring of the physical state of nanosuspensions, and their dissolution, is therefore key to the study of cellular uptake.

Cellular uptake of block copolymer micelle drug delivery vehicles was investigated by Cheng and co-workers[22] using fluorescence (Förster) resonance energy transfer (FRET).[23] FRET relies upon non-radiative energy transfer (long-range, <10 nm, dipole–dipole coupling) from a donor fluorophore in an electronic excited state to a second fluorophore, the acceptor. A FRET signal is observed when the donor molecule is excited and transfers its energy to the acceptor, resulting in acceptor emission.

The micelles were loaded with a pair of FRET dyes (donor and acceptor) and were considered intact if a FRET signal was observed, indicating close proximity of the donor and acceptor fluorophores within the hydrophobic interior of the micelle. Decomposition of the micelles, or release of dye from the micelle, caused a loss in the FRET signal as the two fluorophore molecules became dissociated resulting in loss of energy transfer. We were interested in using the same concept to monitor the physical state of the particles during cellular uptake, however, traditional top-down approaches used to produce nanosuspensions (such as milling or high-pressure homogenization) are not suitable for producing nanoparticles that contain two different organic molecules.

In this paper we use a simple modified emulsion-templated freeze-drying method[24] to produce a dual-component hydrophobic nanosuspension where the particles contain a FRET fluorophore pair. We demonstrate that these particles indeed contain both fluorophores and that dissolution of the particles is accompanied by dramatic reduction in the FRET signal. These particles were used to investigate cellular uptake into human monocyte derived macrophages (activated THP-1 cells (A-THP-1)) and Caco-2 cells before assessing the permeability of these particles through a Caco-2 cell monolayer.

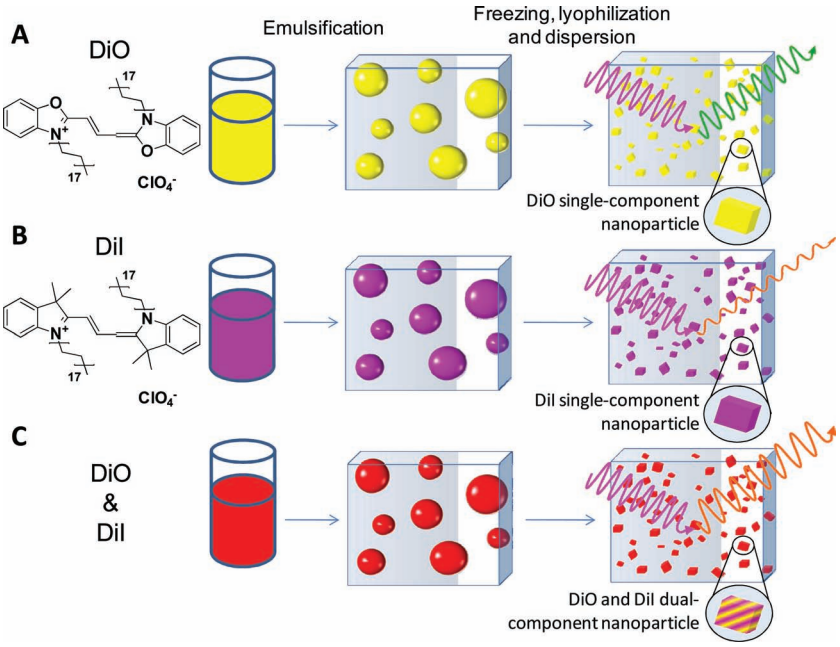

Figure 1. Schematic representation of single and dual-component fluorescent nanosuspension production. Fluorophores were dissolved in chloroform and emulsified in an aqueous solution containing surfactant and a polymer stabilizer. The emulsions were then cryogenically frozen and lyophilized to yield an emulsion-templated porous solid. Upon dispersion into water, the porous solids form nanosuspensions of solid fluorescent nanoparticles. A) Production of a DiO single-component nanosuspension; B) production of a DiI single-component nanosuspension; and C) production of a DiO and DiI dual-component nanosuspension.

2. Results and Discussion

2.1. Nanosuspension Synthesis and Characterization

Single component, containing one fluorophore, and dual-component, containing both acceptor and donor fluorophores, nanosuspensions were prepared by a modified emulsion-templated freeze-drying method (**Figure 1**). Briefly, 3,3′-dioctadecyloxacarbocyanine perchlorate (DiO) and 1,1′-dioctadecyl-3,3,3′,3′-tetramethylindocarbocyanine perchlorate (DiI) were dissolved in chloroform either individually or together in various ratios. The chloroform solutions were emulsified with an aqueous solution containing a non-ionic polyethylene oxide hexadecyl ether surfactant (Brij 58) and 80% hydrolyzed polyvinyl alcohol (PVA). After immediate freezing of the emulsions in liquid nitrogen the samples were lyophilized, removing the water and chloroform to yield a porous solid. Addition of water to the products resulted in dissolution of the water-soluble polymer/surfactant matrix and release of the hydrophobic fluorophores as stabilized nanosuspensions.

Analysis of the single component and dual-component dispersions by dynamic light scattering (DLS) showed monomodal distributions with similar mean sizes (**Figure 2**A). The *z*-average diameters of the nanosuspensions were 184 nm, 123 nm, and 165 nm (±9 nm) with polydispersity indexes (both defined in ISO13321) of 0.265, 0.255 and 0.228 (±0.07) for single-component DiO, single-component DiI, and DiO_{50}/DiI_{50} dual-component particles, respectively. Additionally, the nanosuspensions were stable for at least 1 month with average size and distribution remaining unchanged (Supporting Information, Figure 1S). Zeta potential measurements of the nanosuspensions also indicated similar values which appeared to be largely independent of composition (10–12 mV ±4 mV), the minor cationic charge of the nanosuspensions arising from DiO and DiI. The low zeta potentials suggest that colloidal stability was given by the steric stabilization from adsorbed PVA and the overall similarity of the particles was considered appropriate for direct comparative studies. The nanoparticles were imaged using a graphene oxide (GO) support. Previous reports

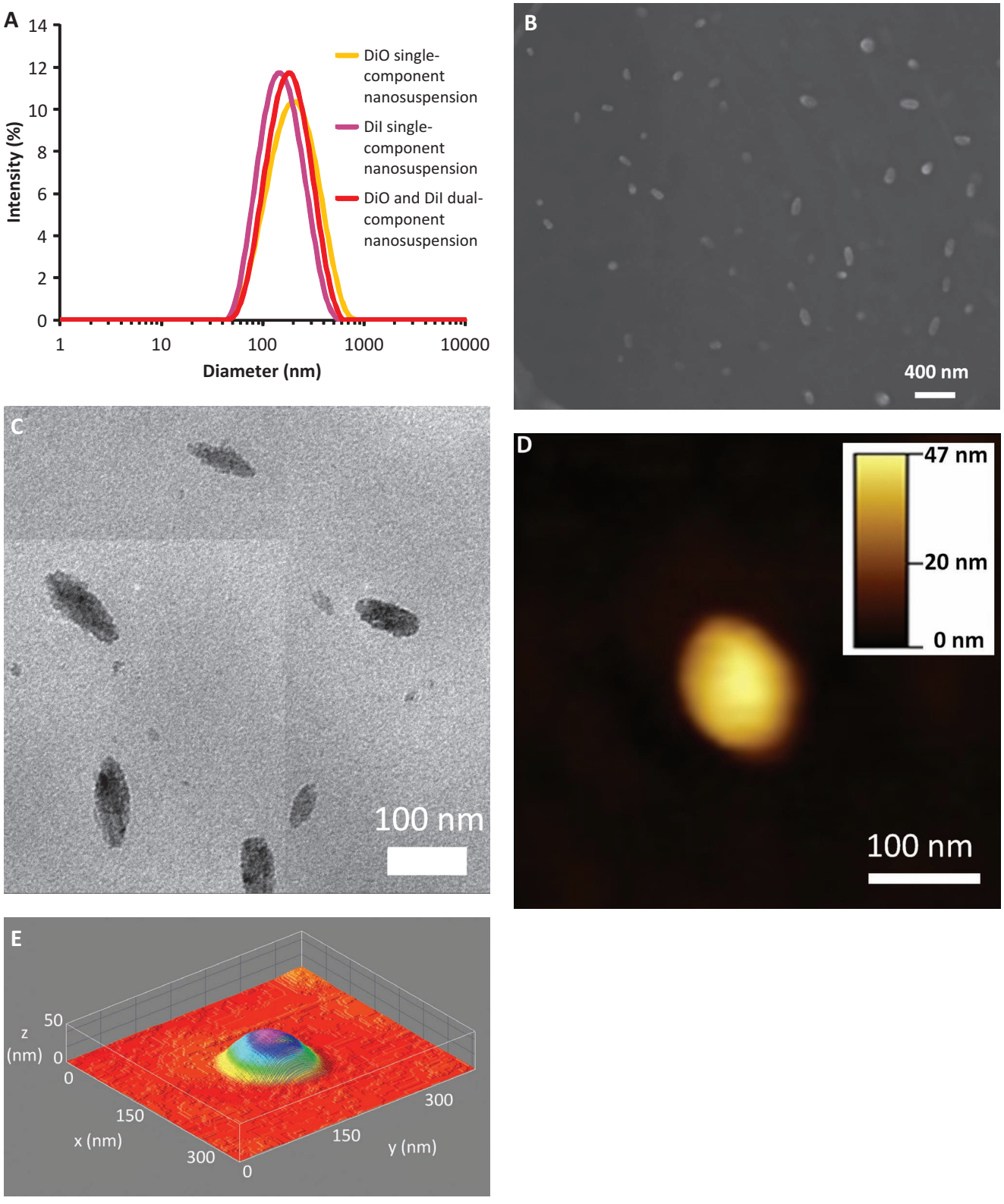

Figure 2. Physical characterization of fluorescent nanoparticles. A) DLS analysis (intensity weighted size distribution) of the three nanosuspensions (at nanoparticle concentrations of 1 mg mL^{-1}); DiO single-component (orange), DiI single-component (purple) and DiO_{50}/DiI_{50} dual-component (red). B) SEM image of the DiO_{50}/DiI_{50} dual-component particles. C) TEM image of DiO_{50}/DiI_{50} dual-component particles. D) AFM image of a single DiO_{50}/DiI_{50} dual-component particle. E) Surface plot of the particle in the AFM image.

have demonstrated the advantages of using GO as a low contrast support for transmission electron microscopy (TEM)[25–28] and recently as a support for multi-technique imaging by TEM, scanning electron microscopy (SEM) and atomic force microscopy (AFM).[29] The three techniques can be performed concurrently on the same GO-grid, simplifying the collection of complementary images. Furthermore the nature of the GO grid allows for images to be collected unstained and uncoated, minimizing misinterpretation of data and allowing for more accurate correlation of results. The morphology of the particles was first examined by TEM and SEM (Figure 2B,C) and irregular, asymmetric shapes with a high aspect ratio were observed using both techniques. Characterization of the particles by AFM (Figure 2D,E) yielded a similar morphology; flattened asymmetric particles in the same size range as determined by SEM and TEM. Although the sizes determined by TEM, SEM, and AFM appear to be smaller than the DLS measurements, all values are consistent in showing the formation of <200 nm particles, especially when considering the approximation to spheres that is inherent in DLS measurement. Analysis of the materials by X-ray powder diffraction (XRPD) revealed that the particles were composed of the fluorophores in an amorphous state (Supporting Information Figure 2S).

2.2. Characterizing Nanosuspension Fluorescence and FRET Emission

FRET is a well-established method used primarily to study protein interactions and conformation changes in situ.[30] FRET occurs when two fluorophores with an overlap in their emission and excitation are within close proximity (less than 10 nm). FRET is observed as a decrease in the donor emission along with a concomitant increase in the emission of the acceptor occurring through the energy transfer from donor to acceptor. An unequivocal FRET signal therefore clearly demonstrates the presence of dual-component nanoparticles, i.e., single particles containing both fluorophores.

DiO and DiI are a well reported FRET fluorophore pair and excitation of DiO at relatively low wavelengths will result in emission from DiI if the dyes are located within close proximity (**Figure 3**E). In order to verify the occurrence of FRET, and therefore the co-localization of the two fluorophores within single combination particles, fluorescence spectra of both single and dual-component nanoparticles were obtained (Figure 3). An excitation wavelength ($\lambda^{DiO}{}_{ex}$) of 420 nm was found to give good discrimination between DiO and DiI single-component nanosuspensions (Supporting Information Figure 5S); we found no effect on the emission peak wavelength when varying the excitation wavelength of any of the fluorescent nanosuspensions, therefore no red-edge excitation shift[31,32] was observed. The single-component nanosuspension of DiO showed a peak emission ($\lambda^{DiO}{}_{em}$) at 545 nm (Figure 3A), while the single-component nanosuspension of DiI displayed a weak emission ($\lambda^{DiI}{}_{em}$) at 598 nm (Figure 3B) due to poor excitation efficiency at 420 nm. Dual-component DiO_{50}/DiI_{50} nanosuspensions exhibited a single strong emission $\lambda^{DiI}{}_{em}$ peak (598 nm) when excited at 420 nm (Figure 3C) and no emission at 545 nm. The absence of a $\lambda^{DiO}{}_{em}$ peak and the presence of a sole $\lambda^{DiI}{}_{em}$ peak when

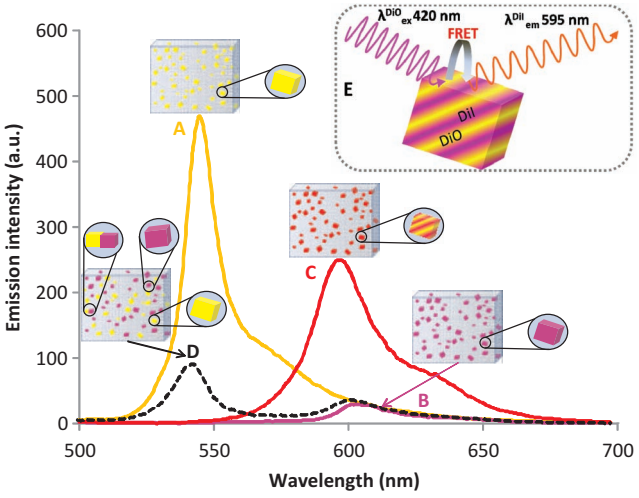

Figure 3. Fluorescence emission spectra of different nanosuspensions obtained upon excitation at 420 nm (at an overall nanoparticle concentration of 0.032 mg mL^{-1}): A) DiO single-component nanosuspension (yellow); B) DiI single-component nanosuspension (purple); C) DiO_{50}/DiI_{50} dual-component nanosuspension (red; FRET ratio = 0.98); and D) 1:1 mixture of both single-component DiO and single-component DiI nanosuspensions (0.016 mg mL^{-1} of DiO nanosuspension and 0.016 mg mL^{-1} of DiI nanosuspension (total fluorophore concentration 0.032 mg mL^{-1})), (black dotted line; FRET ratio 0.30). E) A scheme for the FRET signal from the dual-component nanoparticles.

exciting the nanosuspension at $\lambda^{DiO}{}_{ex}$ corresponds to efficient energy transfer between the two fluorophores. The extent to which FRET occurs may be quantified using the FRET ratio $I_{DiI}/(I_{DiO} + I_{DiI})$, where I_{DiO} and I_{DiI} are the fluorescence intensities at 545 and 598 nm respectively when exciting the nanosuspensions at $\lambda^{DiO}{}_{ex}$ (420 nm). The DiO_{50}/DiI_{50} dual-component nanosuspension displayed a FRET ratio of 0.98; almost complete energy transfer.

The potential for the FRET behavior originating from the close proximity of separate particles of each fluorophore was studied by measuring the fluorescence of a 1:1 mixture of single component nanosuspensions of DiO and DiI (Figure 3D). Two distinct emission peaks at 540 and 598 nm were observed when the mixture was excited at 420 nm (FRET ratio of 0.30) indicating a low level of energy transfer occurring between the fluorophores when in separate particles and supporting the presence of DiO and DiI within the dual-component nanoparticles.

The relative ratio of the donor to acceptor fluorophore within the dual-component particles was readily varied using the emulsion-templated freeze-drying nanoparticle synthesis. Dual-component particles ranging in mean diameters between 120–255 nm were produced over a range of compositions from 100% DiO to 100% DiI. As the relative amount of DiO in the dual-component particles was increased, the average particle diameter in the dispersions was found also to generally increase (Supporting Information Figure 3S) at a constant PVA/Brij 58/total fluorophore ratio (wt%). Analysis of the fluorescence emission (**Figure 4**A) of dual-component nanosuspensions with varying DiO/DiI ratios showed that very low additions of acceptor (e.g., DiO_{90}/DiI_{10}) yielded a large increase in acceptor emission and subsequent decrease in donor emission (with a FRET ratio of 0.87). Further increases in the DiI content resulted in

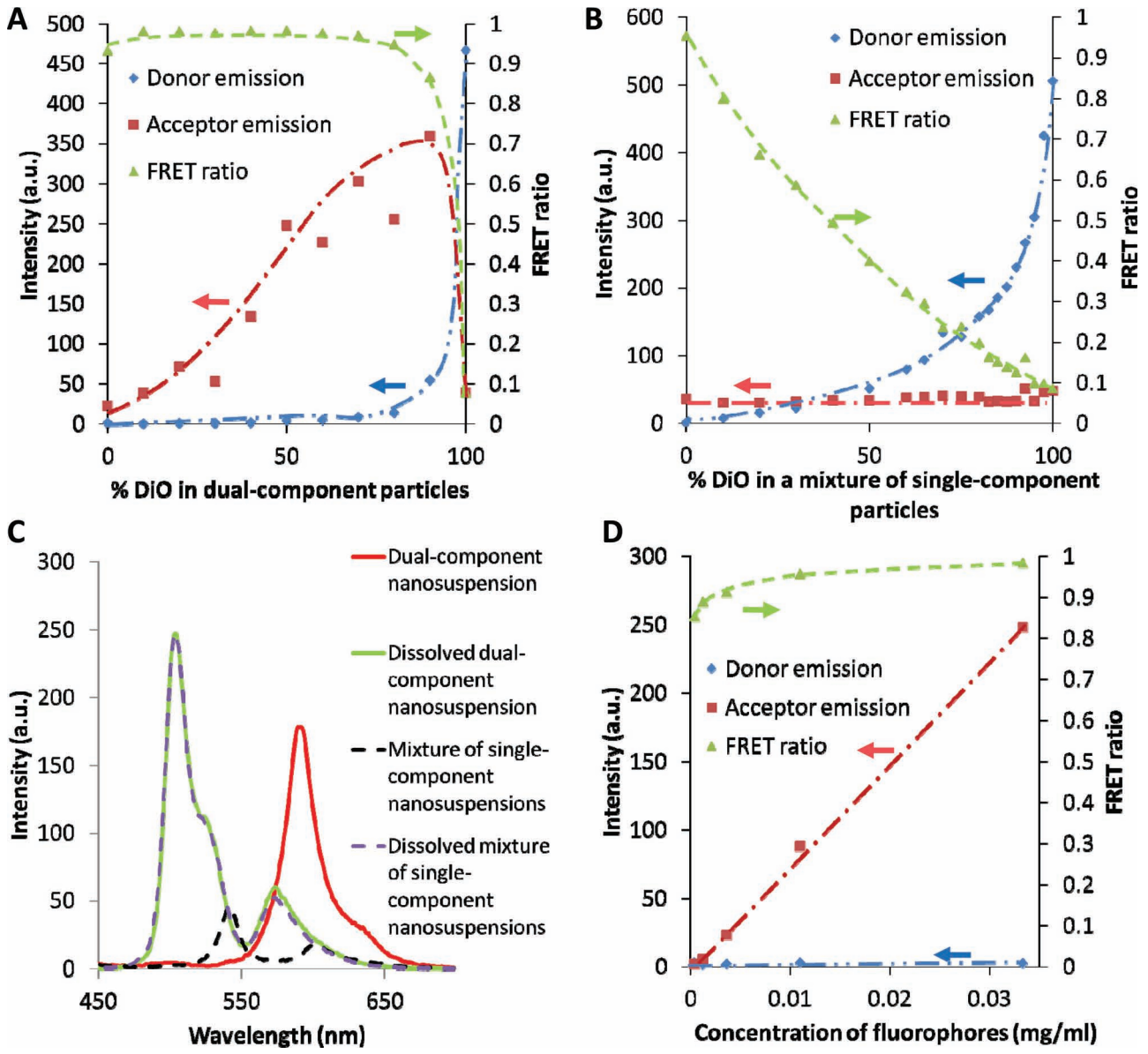

Figure 4. Fluorescence characterization of single and dual-component nanosuspensions upon excitation at λ^{DiO}_{ex} (420 nm): A) effect of varying the ratio of DiO to DiI on fluorescent emission of dual-component nanosuspension (nanoparticle concentration of 0.032 mg mL^{-1}); B) effect of varying the ratio of DiO to DiI on fluorescent emission of a mixture of single-component nanosuspensions of DiO and DiI (total nanoparticle concentration of 0.032 mg mL^{-1}); C) fluorescent emission spectra of DiO_{50}/DiI_{50} dual-component nanosuspensions in water (red line; FRET ratio 0.98), DiO_{50}/DiI_{50} dual-component nanosuspensions in methanol (green line; FRET ratio 0.17), a 1:1 mixture DiO and DiI single-component nanosuspensions in water (black dotted line; FRET ratio 0.30) or a 1:1 mixture DiO and DiI single-component nanosuspensions in methanol (purple dotted; line; FRET ratio 0.19). The total fluorophore concentrations were 0.016 mg mL^{-1} for all four spectra; D) Effect of dilution on the fluorescent emission of the DiO_{50}/DiI_{50} dual-component nanosuspension.

decreasing acceptor emission possibly due to increased self-quenching within the solid nanoparticles. Increasing the DiI content to DiO_{70}/DiI_{30} yielded spectra with complete absence of the donor emission when the nanosuspensions were excited at λ^{DiO}_{ex}; thus all energy is transferred to the acceptor, DiI (a FRET ratio of 0.97). As a FRET ratio is defined as the acceptor emission divided by the sum of acceptor and donor emission, we have calculated FRET ratios across all compositions, understanding that a FRET ratio of a single-component nanosuspension of DiI will have a value very close to 1, similarly a single-component DiO nanosuspension has a value very close to zero. These values are clearly not derived from FRET however this approach allows comparison across the full composition range available. Varying the ratio of individual DiO particles to DiI particles in a mixture of the single-component nanosuspensions led to completely different behavior (Figure 4B). Acceptor emission was not found to increase at any ratio of DiO/DiI, probably due to the isolation of donor

and acceptor within individual particles. The potential for FRET is therefore restricted to either a) surface contact of the nanoparticles or b) energy transfer between the low concentrations of dissolved molecules of DiO and DiI (either in solution or within surfactant/polymer assemblies). The observed increase in FRET ratio (with increasing DiI content) is purely related to the subsequent reduction in DiO at increased DiI levels (to maintain constant total fluorophore concentration) and resulting decreased DiO emission.

Particle breakdown or dissolution may also be observed by monitoring the FRET signal from the dual-component nanoparticles. As the particles begin to dissolve the two fluorophores are no longer co-localized within the particles and the distance between the donor and acceptor increases. For example, after dissolution of the DiO_{50}/DiI_{50} dual-component nanosuspension in methanol, FRET was found to be greatly reduced (Figure 4C) with the FRET ratio (the wavelengths chosen to represent the two fluorophores are adjusted to account for blue shift) reduced from 0.98 in water to 0.19 as a dissolved solution. Additionally, DLS analysis of the methanol solutions did not yield sufficient scattering for accurate size measurement, providing further evidence that particle dissolution had occurred. When a similar methanol dissolution was performed on a mixture (1:1) of DiO and DiI single-component dispersions, nearly identical fluorescence spectra were observed, supporting our conclusions that the observed FRET signal from the single nanoparticle mixtures arises from low level energy transfer at the molecular or particle surface level. Blue shifting of the emission was observed for both DiO (–39 nm) and DiI (–28 nm) along with an increase in emission intensity upon dissolution. This finding was likely due to separation of fluorophores within the excimer assemblies present within the nanoparticles and a subsequent loss of self-quenching.[33] The dramatic reduction in FRET and FRET ratio during dual-component nanoparticle dissolution provides a useful measure allowing monitoring of the physical state of the nanosuspensions.

In order to verify that the dual-component nanosuspensions can be used at the appropriate concentrations for cellular uptake studies, serial dilution experiments were carried out using the DiO_{50}/DiI_{50} dual-component nanosuspension to determine whether, at such low concentrations, nanoparticle dissolution would occur. (Figure 4D). The FRET signal (acceptor emission from excitation at λ^{DiO}_{ex}) decreased in a linear manner as the nanosuspensions were diluted. The apparent decrease in the FRET ratio at very high dilutions was due to the very low acceptor emission relative to the noise in the measurement of the donor emission. The data suggest limited dual-component nanosuspension dissolution in the low concentration range required for cellular uptake and transport measurements using fluorescence spectroscopy. The dual-component nanoparticles are therefore useful probes for cellular uptake/transport experiments, allowing the combined spatial reporting and indication of physical state of the nanoparticles within the experiment.

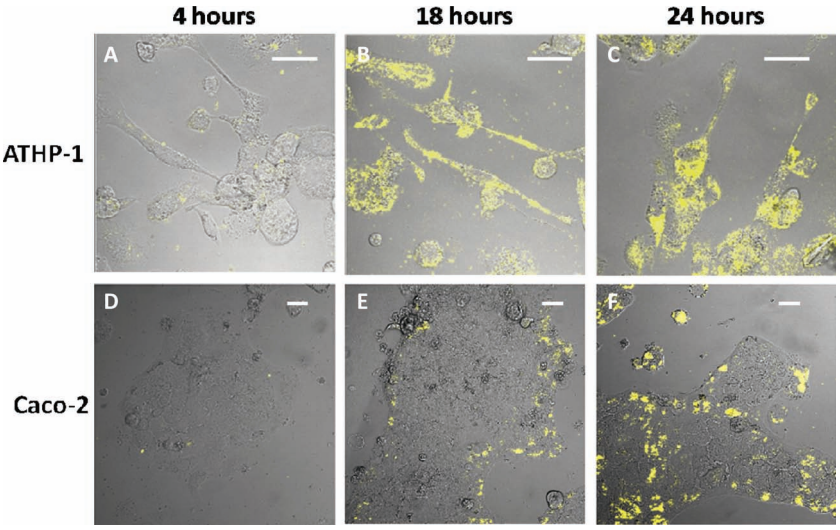

Figure 5. Confocal fluorescence microscopy of A-THP-1 and Caco-2 cells exposed to dual-component nanosuspensions (14 μM fluorophore concentration) at three different incubation times. FRET emission from the dual-component nanosuspensions is represented in yellow. (Scale bars are 40 μm).

2.3. Analysis of Cellular Uptake by Confocal Fluorescence Microscopy

To investigate cellular uptake of the dual-component particles, A-THP-1 macrophages, and Caco-2 intestinal cells were each incubated with dual-component nanosuspensions at 0.0125 mg mL^{-1} (14 μM fluorophore concentration) for 24 h. Confocal fluorescence microscopy was utilized to visualize the cells during the 24 h exposure (**Figure 5**) and after 18 h, dual-component particles had clearly been internalized by the A-THP-1 cells (Figure 5B). There was no visual evidence of aggregation of the nanosuspensions in the bulk media and separate DLS measurements of the nanosuspension in media confirmed no increase in particle size (Supporting Information Figure 6S). Although the mechanism of cellular uptake requires further investigation, a putative hypothesis is phagocytosis. Observation of Caco-2 cells showed very limited internalization of nanoparticles (Supporting Information Figure 8S) with the majority of particles adhered to the cell surface (Figure 5E,F). While, cellular uptake of nanoparticles into Caco-2 cells has been shown in the literature,[34–36] it also been reported to be highly dependent on a range of factors including size,[34,37] shape,[37] hydrophilicity,[35] and composition.[35] The low levels of uptake into Caco-2 cells, for the dual-component particles, was surprising however may be driven by a combination factors specific to our particles (e.g., the elongated shape and surface charge). The apparent differences in cellular uptake supports the hypothesis that the primary internalization mechanism is phagocytosis as Caco-2 cells are not phagocytic.[21]

Full spectral analysis (lambda scan) of the emission of individual pixels within the confocal microscopy images allows quantification of the FRET ratio. This reports the physical state of the DiO_{50}/DiI_{50} dual-component nanoparticles in the A-THP-1 cells (**Figure 6**A,B). The emission spectra at a number of representative regions of interest (ROI) (up to 11

ROIs) inside the cells showed a clear difference between dual-component nanoparticles and the corresponding 1:1 mixture of DiO and DiI single-component nanoparticles (Figure 6A,C). Very little donor emission, $\lambda^{DiO}_{em,}$ was observed for the DiO_{50}/DiI_{50} dual-component nanoparticles indicating that the particles were internalized intact throughout the exposure. However, the 1:1 mixture of DiO and DiI single-component nanoparticles displayed a clear donor emission (λ^{DiO}_{em}) at 537 nm, slightly blue-shifted from the bulk measurements (Figure 3A) of 545 nm potential evidence of some dissolution of the DiO single-component nanoparticles. Interestingly, the mixture of DiO and DiI single-component nanoparticles also showed reduced donor emission inside the cell compared to the initial mixture of nanosuspensions (Supporting Information Figure 11S B). This indicates that the single-component donor and acceptor nanoparticles had been individually internalized and appear to accumulate within close proximity in the same regions of the cell. The FRET ratio (after 24 h) was found to be significantly (with a p-value of 0.046) higher for the dual-component particles (0.89; Figure 6D) than for the mixture of single-component particles (0.74; Figure 6E). pH studies of the dual-component nanosuspensions in the absence of cells (Supporting Information Figure 12S), showed identical fluorescence spectra over a range of pH values (4.8–8.9). Investigation of the FRET ratios over the three time points showed that the FRET ratios remained constant over time for both dual-component (Figure 6F) and the mixture of single-component nanoparticles (Figure 6G), while the single-component particles seemed to display slightly greater accumulation. Comparison of the FRET ratios from within the cell (after 24 h) against those of the aqueous dispersion (Supporting Information Figure 11S C) showed that the dual-component nanoparticles may have undergone slight particle dissolution as the FRET ratio decreased from 0.97 to 0.89. Overall, these findings provide strong evidence that the dual-component nanoparticles are internalized into A-THP-1 cells as intact structures with only minor dissolution.

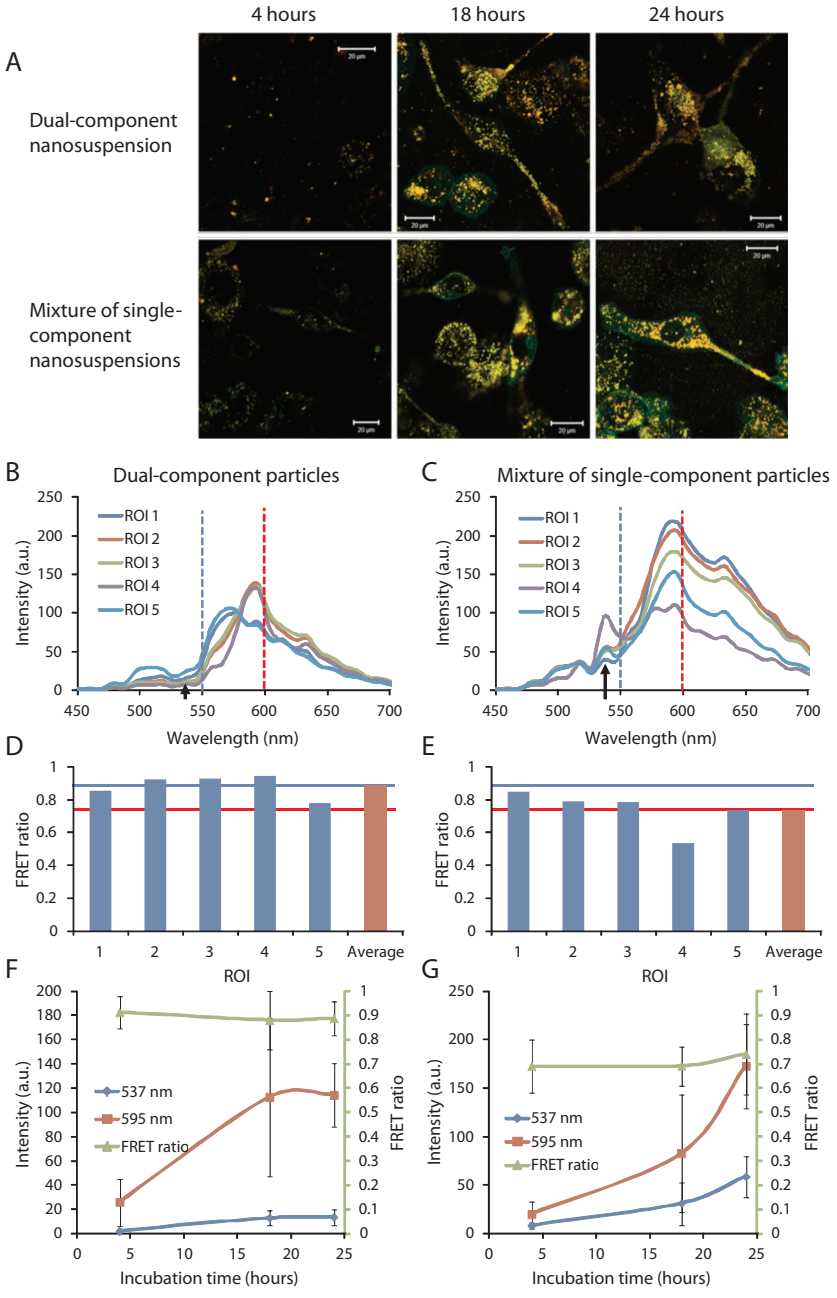

Figure 6. Confocal fluorescence microscopy analysis of A-THP-1 cells incubated with either a dual-component nanosuspension (DiO_{50}/DiI_{50}) or a 1:1 mixture of single-component nanosuspensions (14 μM fluorophore concentration) (corresponding brightfield images Supporting Information Figure 11S): A) confocal lambda scan of A-THP-1 cells incubated with a dual-component nanosuspension (upper) or a mixture of single-component nanosuspensions (lower) (the scale bars are 20 μm); B,C) spectral analysis of five ROIs within cells (all the ROIs selected are shown in Supporting Information Figure 8S), arrows indicate λ^{DiO}_{em} (537 nm). Individual ROI FRET ratios for D) accumulated dual-component nanoparticles (blue line shows average across ROIs) and E) accumulated mixture of single-component nanoparticles (red line shows average across ROIs); Monitoring of fluorescence of accumulated nanoparticles during incubation of cells with F) dual-component nanosuspension and G) mixture of single-component nanosuspensions; emission intensities of the donor (537 nm) and acceptor (595 nm) and FRET ratios are shown as the mean from the ROIs

Transport of organic nanoparticles through Caco-2 cell monolayers was studied. This model has tight junctions and a luminal (apical) and systemic compartment (basolateral) mimicking the gut and blood, respectively.[38] DiO_{50}/DiI_{50} dual-component nanosuspensions were compared to a 1:1 mixture of DiO and DiI single-component nanosuspensions by addition to the apical compartment at a concentration relevant to in vivo drug particles dosed orally (50 μM). After 18 h the basolateral chamber

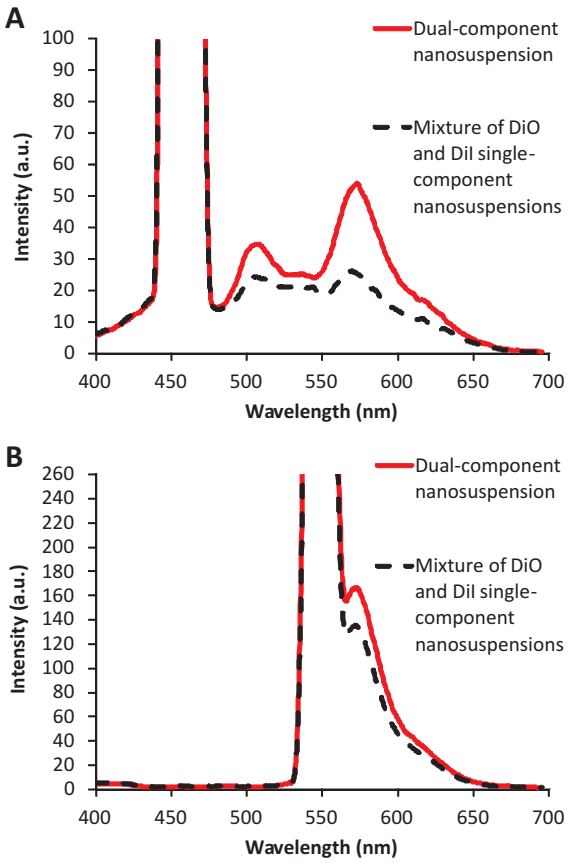

Figure 7. Fluorescent emission spectra of DiO_{50}/DiI_{50} dual-component nanosuspensions and the 1:1 mixture of DiO single-component and DiI single-component nanosuspensions after transport through Caco-2 cell monolayer (incubated at 50 μM fluorophore concentration). A) Emission spectra of nanosuspensions with an excitation wavelength of 458 nm (λ^{DiO}_{ex}). B) Emission spectra of nanosuspensions with an excitation wavelength of 550 nm (λ^{DiI}_{ex}).

(systemic circulation mimic) was sampled and analyzed by fluorimetry (**Figure 7**) to quantify the concentration of fluorophore that had transported through the monolayer. The low concentrations of fluorophore detected in the basolateral chamber indicated a low level of transport and required an excitation wavelength of 458 nm to increase overall emission from the samples. This wavelength provides less discrimination between FRET and DiI excitation/emission but this compromise was necessary to increase sensitivity and allow accurate fluorophore quantification.

The emission spectra (Figure 7A) of the basolateral compartment after 18 h showed an observable fluorescence when applying either the dual-component or mixture of single-component nanosuspensions to the apical compartment. Two specific peaks were observed in the spectra, one at approximately 505 nm, corresponding to DiO emission, and a second peak at approximately 575 nm assigned to DiI emission. In both cases, the dual-component and mixture of single-component nanosuspensions displayed blue shifted spectra (similar λ_{max} values as those observed in methanol) suggesting the presence of a majority of dissolved molecules after permeation. The emission spectra from the basolateral samples when using dual-component nanosuspensions displayed a noticeably stronger emission for both DiO and DiI (FRET ratio = 0.61) than samples taken when using a mixture of single-component nanosuspensions (FRET ratio = 0.52). The observed FRET ratio however provides no accurate quantification of the levels of fluorophore that has transported. To understand the physical nature of the nanosuspensions during transport it is important to quantify the acceptor fluorophore individually by using a second excitation wavelength of 550 nm (Figure 7B). The wavelength and emission intensity of DiI was approximately equal for both the dual-component and the single-component nanosuspensions, implying that the same amount of DiI fluorophore had passed through the cell monolayer into the receiver well. The differences in FRET ratio (excitation at 458 nm) are therefore derived from the proximity of DiO and DiI in the basolateral chamber which suggests that at least some of the dual-component nanoparticles crossed the cell monolayer as intact particles; DiO and DiI permeating together in a single nanoparticle. The observation of a FRET signal in the basolateral compartment, (Figure 7A) coupled with the low level of intracellular FRET signal in Caco-2 cells from our accumulation studies, (Supporting Information Figure 8S) would also indicate that the nanoparticles may have traversed the monolayer via a paracellular route, between the cells, rather than by permeation through the cell. Paracellular movement of nanoparticles has been shown previously,[39] in the presence of chitosan either as particles or as dissolved molecules, enhancing drug transition through Caco-2 monolayers.[40–42] It has been suggested that chitosan, carrying a permanent positive charge, causes reversible opening in the paracellular channels due to electrostatic interactions resulting in disruption of the tight junctions.[42,43] It is possible that the cationic character of our dual-component nanoparticles led to a similar disruption within the tight junctions. The potential for paracellular movement of the nanoparticles presented here is not completely intuitive, as our particles contain no chitosan. Further study, which may add considerable understanding to the enhanced bioavailability and pharmacokinetics observed for many nanosuspension medicines, is therefore required.

3. Conclusions

Unlike previous nanosuspension techniques, we have controllably generated a range of single-component and dual-component fluorescent nanoparticles (<200 nm) with varying composition using an emulsion-templated freeze-drying method. By selecting a FRET-pair of fluorophores, we were able to determine the different fluorescence properties of mixtures of single component nanosuspensions and dual-component nanoparticles. The highly efficient FRET observed within the dual-component nanosuspensions allows the reporting of nanoparticle physical state using conventional fluorescence microscopy. The application of the dual-component nanosuspensions to cellular uptake studies have demonstrated particle localization within or at the surface of the cells studied and the presence of intact particles within macrophages after only 4 h incubation. Limited internalization of nanoparticles was seen within Caco-2 cells but permeation experiments suggested the

potential for paracellular transport of nanoparticles across an epithelial monolayer with tight junctions. The passage of intact nanoparticles across intestinal epithelial cells has implications that require further study as this may clarify mechanisms of modified in vivo behavior of current and potential nanoparticle therapies.

4. Experimental Section

Materials: Unless stated otherwise, all of the reagents and solvents were used as received. 3,3′-dioctadecyloxacarbocyanine perchlorate (DiO) and 1,1′-dioctadecyl-3,3,3′,3′-tetramethylindocarbocyanine perchlorate (DiI) were purchased from Invitrogen. Poly(vinyl alcohol) (PVA; 80% hydrolyzed, MW 9000–10 000), Brij 58, RPMI-1640, phorbol 12-myristate 13 acetate (PMA) and Dulbecco's modified Eagle's medium (DMEM) were purchased from Sigma-Aldrich.

Particle Synthesis: Particles were prepared by emulsion templating followed by freezing and lyophilization. DiO or DiI were dissolved in chloroform at 10 mg mL^{-1}. 100 µL of DiO or DiI solution (or 50 µL of DiO and 50 µL DiI for the dual-component particles) was added to a 3 mL vial. 133 µL of Brij 58 (22.5 mg mL^{-1} in DI water) and 267 µL of PVA (80% hydrolyzed) (22.5 mg mL^{-1} in DI water) were added to this organic solution. An emulsion was formed by sonicating the sample for 12 s using a Covaris S2x with a duty cycle of 20, an intensity of 10 and 500 cycles per burst in frequency sweeping mode. The samples were then immediate frozen in liquid nitrogen. Lyophilizing for three days (Virtis benchtop K) yielded a porous solid that upon addition of water produced a nanosuspension.

Particle Characterization: The average size and zeta potential of the nanosuspensions were measured at 1 mg mL^{-1} at a temperature of 25 °C using a Malvern Zetasizer Nano ZS equipped with a 4 mW He-Ne, 633nm laser. The z-average diameters and polydispersity indexes were obtained by DLS. Malvern Zetasizer software version 6.20 was used for data analysis. Zeta potential measurements were also carried out at 1 mg mL^{-1}, at 25 °C, a pH of 6.5, using disposable capillary zeta cells. The fluorescence spectra of the nanoparticle dispersion were obtained on a PerkinElmer LS55 using disposable UV-grade PMMA cuvettes with a path length of 1 cm. For fluorescence spectrometry the emulsion-templated solids were dispersed in deionised water to a fluorophore concentration of 0.032 mg mL^{-1}. For the dissolution in methanol experiments the solids were first dispersed in water at 1 mg mL^{-1}, which was then dissolved in methanol to a concentration of 0.016 mg mL^{-1}. The excitation and emission slits were unchanged when measuring spectra that were directly compared and no normalization of the data was carried out.

Electron Microscopy: Prior to electron microscopy the dual-component sample (DiO_{50}/DiI_{50}) was dialyzed for 4 days using a biodialyzer fitted with cellulose acetate membranes with a molecular weight cut-off of 50 000 daltons (Harvard Apparatus) (dialysis was found to have no effect on particle size (Supporting Information Figure 4S)). All electron microscopy images were obtained with the sample deposited on a modified TEM grid, these were prepared as follows: Solutions of graphene oxide[28] were synthesized as previously reported. GO solutions (0.10–0.15 mg mL^{-1}) were sonicated for 30 s prior to use. Lacey carbon grids (400 Mesh, Cu) (Agar Scientific) were cleaned using air plasma from a glow-discharge system (2 min, 20 mA). One drop (≈0.08 mL) of the sonicated GO solution was deposited onto each grid and left to air-dry for ≈30 min. 4 µL of sample (at 0.5 mg mL^{-1}) was pipetted onto a GO grid and blotted immediately blotted away using a piece of filter paper. TEM images were recorded on either a JEOL 2000FX TEM or a JEOL 2100 equipped with Gatan Orius digital camera, both were operated at 200 kV. While, a Zeiss Supra55VP was used to acquire the SEM images, operated at an accelerating voltage of 20 kV.

Atomic Force Microscopy (AFM): AFM images were taken in tapping mode on a Multimode AFM with Nanoscope IIIA controller with Quadrex. Silicon AFM tips were used with nominal spring constant and resonance frequency of 3.5 Nm^{-1} and 75 kHz (MikroMasch NSC18). ImageJ 1.44 with the interactive 3D surface plot plugin was used to produce the AFM surface plot.

Routine Cell Culture: Caco-2 cells were purchased from American Type Tissue Culture (ATCC: USA) and THP-1 cells were purchased from European Collection of Cell Cultures (ECCAC; Porton Down, UK). Caco-2 cells were routinely maintained in DMEM supplemented with 15% fetal bovine serum (FBS; BioWhittaker, Berkshire, UK) and THP-1 cells were grown in RPMI-1640 supplemented with 10% FBS. Both cell lines were incubated at 37 °C and 5% CO_2 and Caco-2 cells were sub-cultured every 4 days. THP-1 cells were sub-cultured when a density of 1×10^6 cells mL^{-1} was achieved, prior to being seeded at a density of 2.5×10^4 mL^{-1} into 12 wells of an Iwaki 24 well glass bottomed plate (Asahi Glass Co; Japan). Activation of THP-1 cells into macrophage-like cells (A-THP-1) was accomplished by addition of phorbol 12-myristate 13 acetate (PMA; 10nM) and incubation at 37 °C and 5% CO_2 for 7 days. Caco-2 cells were seeded at a density of 2.5×10^4 mL^{-1} into the remaining 12 wells of an Iwaki 24 well glass bottomed plate and allowed 24 h to adhere.

Confocal Microscopy: The emulsion-templated solids were dispersed in deionised water to a fluorophore concentration of 1.0 mg mL^{-1}. These dispersions were then diluted with the appropriate cell specific media (i.e., RPMI-1640 and 10% FBS for A-THP-1 or DMEM supplemented with 10% FBS for Caco-2) to 0.0125 mg mL^{-1} (14 µM fluorophore concentration). A-THP-1 cells were then incubated with either dual-component particles with a DiO:DiI ratio of 1:1, whereas Caco-2 cells were incubated with dual-component particles with a DiO:DiI ratio of 7:3. Images were obtained by confocal laser scanning microscopy at 4, 18, and 24 h after addition of the nanosuspensions. A Zeiss LSM510 or a Zeiss LSM710 on a Zeiss Observer Z1 (Zeiss, Jena, Germany) were used for imaging. The nanosuspensions were excited using an argon ion laser at 458 nm and detected with a Zeiss Meta detector. In the confocal channel images (Figure 5) a spectral filter of 570–673 nm was used FRET emission. For the spectral analysis the emission between 500–700 nm was collected at 10 nm intervals. Data was captured using Zeiss Zen software (Zeiss, Jena, Germany) and analyzed using Zeiss LSM image browser (version 4,2,0,121).

Transwell Experiment: Caco-2 cells were inoculated (4×10^4 cells per well) onto Corning 24 Well HTS Transwell support plates (Corning Ltd.) and allowed to propagate, differentiate, and polarize over a 21 day period as previously described,[38] where the cell media (DMEM containing 15% FBS) was replaced every other day. The emulsion-templated solids were dispersed in deionised water to a fluorophore concentration of 1.0 mg mL^{-1}. These nanosuspensions were then diluted to 50 µM in Hanks buffer containing 0.5 mM L-glutamine. These nanosuspensions were added to the apical compartment (intestinal lumen mimic) and transcellular permeability was assessed by fluorimetry (PerkinElmer LS55) after pooling the recipient buffer contained in 5 basolateral compartments after 18 h incubation.

Supporting Information

Supporting Information is available from the Wiley Online Library or from the author.

Acknowledgements

The authors wish to thank the RCUK for Grand Challenge Grant Funding (EP/G066272/1) that funded the research. Dr. Dave Adams is thanked for access to his fluorimeter.

Received: December 16, 2011
Published online: March 22, 2012

[1] B. E. Rabinow, *Nat. Rev. Drug Discovery* **2004**, *3*, 785.
[2] Y. C. Wang, D. R. Zhang, Z. P. Liu, G. P. Liu, C. X. Duan, L. J. Jia, F. F. Feng, X. Y. Zhang, Y. Q. Shi, Q. Zhang, *Nanotechnology* **2010**, *21*, 155104.
[3] H. Zhang, C. P. Hollis, Q. Zhang, T. Li, *Int. J. Pharm.* **2011**, *415*, 293.
[4] W. Sun, S. Mao, Y. Shi, L. C. Li, L. Fang, *J. Pharm. Sci.* **2011**, *100*, 3365.
[5] R. Shegokar, M. Jansch, K. K. Singh, R. H. Müller, *Nanomed.: Nanotechnol. Biol. Med.* **2011**, *7*, 333.
[6] N. G. Sahoo, M. Kakran, L. A. Shaal, L. Li, R. H. Müller, M. Pal, L. P. Tan, *J. Pharm. Sci.* **2011**, *100*, 2379.
[7] B. Van Eerdenbrugh, L. Froyen, J. A. Martens, N. Blaton, P. Augustijns, M. Brewster, G. Van den Mooter, *Int. J. Pharm.* **2007**, *338*, 198.
[8] O. Kayser, C. Olbrich, V. Yardley, A. F. Kiderlen, S. L. Croft, *Int. J. Pharm.* **2003**, *254*, 73.
[9] B. Rabinow, J. Kipp, P. Papadopoulos, J. Wong, J. Glosson, J. Gass, C. S. Sun, T. Wielgos, R. White, C. Cook, K. Barker, K. Wood, *Int. J. Pharm.* **2007**, *339*, 251.
[10] E. Lavik, H. von Recum, *ACS Nano* **2011**, *5*, 3419.
[11] F. Kesisoglou, S. Panmai, Y. Wu, *Adv. Drug Delivery Rev.* **2007**, *59*, 631.
[12] R. H. Müller, S. Gohla, C. M. Keck, *Eur. J. Pharm. Biopharm.* **2011**, *78*, 1.
[13] G. Barratt, *Cell. Mol. Life Sci.* **2003**, *60*, 21.
[14] F. Zhao, Y. Zhao, Y. Liu, X. Chang, C. Chen, Y. Zhao, *Small* **2011**, *7*, 1322.
[15] A. Graf, A. McDowell, T. Rades, *Expert Opin. Drug Delivery* **2009**, *6*, 371.
[16] K. L. Aillon, Y. Xie, N. El-Gendy, C. J. Berkland, M. L. Forrest, *Adv. Drug Delivery Rev.* **2009**, *61*, 457.
[17] P. Artursson, J. Karlsson, *Biochem. Biophys. Res. Commun.* **1991**, *175*, 880.
[18] M. P. Desai, V. Labhasetwar, E. Walter, R. J. Levy, G. L. Amidon, *Pharm. Res.* **1997**, *14*, 1568.
[19] S. McClean, E. Prosser, E. Meehan, D. O'Malley, N. Clarke, Z. Ramtoola, D. Brayden, *Eur. J. Pharm. Sci.* **1998**, *6*, 153.
[20] M. Simon, I. Behrens, L. A. Dailey, M. Wittmar, T. Kissel, *Eur. J. Pharm. Biopharm.* **2007**, *66*, 165.
[21] Y. Lai, P.-C. Chiang, J. D. Blom, N. Li, K. Shevlin, T. G. Brayman, Y. Hu, J. G. Selbo, L. G. Hu, *Nanoscale Res. Lett.* **2008**, *3*, 321.
[22] H. T. Chen, S. W. Kim, L. Li, S. Y. Wang, K. Park, J. X. Cheng, *Proc. Natl. Acad. Sci. USA* **2008**, *105*, 6596.
[23] E. A. Jares-Erijman, T. M. Jovin, *Nat. Biotechnol.* **2003**, *21*, 1387.
[24] H. Zhang, D. Wang, R. Butler, N. L. Campbell, J. Long, B. Tan, D. J. Duncalf, A. J. Foster, A. Hopkinson, D. Taylor, D. Angus, A. I. Cooper, S. P. Rannard, *Nat. Nanotechnol.* **2008**, *3*, 506.
[25] N. R. Wilson, P. A. Pandey, R. Beanland, J. P. Rourke, U. Lupo, G. Rowlands, R. A. Romer, *New J. Phys.* **2010**, *12*, 125010.
[26] J. Sloan, Z. Liu, K. Suenaga, N. R. Wilson, P. A. Pandey, L. M. Perkins, J. P. Rourke, I. J. Shannon, *Nano Lett.* **2010**, *10*, 4600.
[27] R. S. Pantelic, J. C. Meyer, U. Kaiser, W. Baumeister, J. M. Plitzko, *J. Struct. Biol.* **2010**, *170*, 152.
[28] N. R. Wilson, P. A. Pandey, R. Beanland, R. J. Young, I. A. Kinloch, L. Gong, Z. Liu, K. Suenaga, J. P. Rourke, S. J. York, J. Sloan, *ACS Nano* **2009**, *3*, 2547.
[29] J. P. Patterson, A. M. Sanchez, N. Petzetakis, T. P. Smart, I. I. I. T. H. Epps, I. Portman, N. R. Wilson, R. K. O'Reilly, *Soft Matter* **2012**, *8*,3322.
[30] B. N. G. Giepmans, S. R. Adams, M. H. Ellisman, R. Y. Tsien, *Science* **2006**, *312*, 217.
[31] A. Chattopadhyay, *Chem. Phys. Lipids* **2003**, *122*, 3.
[32] A. P. Demchenko, *Luminescence* **2002**, *17*, 19.
[33] D.-B. Kim, C.-H. Choi, S.-H. Lee, Y.-S. Lee, K. Zong, S.-C. Yu, *Colloids Surf. A* **2007**, *303*, 201.
[34] M. P. Desai, V. Labhasetwar, E. Walter, R. J. Levy, G. L. Amidon, *Pharm. Res.* **1997**, *14*, 1568.
[35] I. Behrens, A. I. V. Pena, M. J. Alonso, T. Kissel, *Pharm. Res.* **2002**, *19*, 1185.
[36] E. Roger, F. Lagarce, E. Garcion, J. P. Benoit, *J. Controlled Release* **2009**, *140*, 174.
[37] S. Mitragotri, J. Lahann, *Nat. Mater.* **2009**, *8*, 15.
[38] I. Hubatsch, E. G. E. Ragnarsson, P. Artursson, *Nat. Protocols* **2007**, *2*, 2111.
[39] Y.-H. Lin, C.-K. Chung, C.-T. Chen, H.-F. Liang, S.-C. Chen, H.-W. Sung, *Biomacromolecules* **2005**, *6*, 1104.
[40] A. M. M. Sadeghi, F. A. Dorkoosh, M. R. Avadi, M. Weinhold, A. Bayat, F. Delie, R. Gurny, B. Larijani, M. Rafiee-Tehrani, H. E. Junginger, *Eur. J. Pharm. Biopharm.* **2008**, *70*, 270.
[41] D. Vllasaliu, R. Exposito-Harris, A. Heras, L. Casettari, M. Garnett, L. Illum, S. Stolnik, *Int. J. Pharm.* **2010**, *400*, 183.
[42] A. Sadighi, S. N. Ostad, S. M. Rezayat, M. Foroutan, M. A. Faramarzi, F. A. Dorkoosh, *Int. J. Pharm.* **2012**, *422*, 479.
[43] T.-H. Yeh, L.-W. Hsu, M. T. Tseng, P.-L. Lee, K. Sonjae, Y.-C. Ho, H.-W. Sung, *Biomaterials* **2011**, *32*, 6164.